Journal of Power Sources 192 (2009) 486–493

Contents lists available at ScienceDirect

Journal of Power Sources

journal homepage: www.elsevier.com/locate/jpowsour

Global failure criteria for positive/electrolyte/negative structure of planar solid oxide fuel cell

W.N. Liu[a,*], X. Sun[a], M.A. Khaleel[a], J.M. Qu[b]

[a] Pacific Northwest National Laboratory, P.O. Box 999, 906 Battelle Boulevard, Richland, WA 99354, United States
[b] Georgia Institute of Technology, 801 Ferst Dr, Atlanta, GA 30332, United States

ARTICLE INFO

Article history:
Received 29 January 2009
Received in revised form 3 March 2009
Accepted 3 March 2009
Available online 19 March 2009

Keywords:
SOFC PEN
Ceramics
Fracture mechanism
Global fracture criteria
Energy release rate
Critical curvature

ABSTRACT

Due to mismatch of the coefficients of thermal expansion of various layers in the positive/electrolyte/negative (PEN) structures of solid oxide fuel cells (SOFC), thermal stresses and warpage on the PEN are unavoidable due to the temperature changes from the stress-free sintering temperature to room temperature during the PEN manufacturing process. In the meantime, additional mechanical stresses will also be created by mechanical flattening during the stack assembly process. In order to ensure the structural integrity of the cell and stack of SOFC, it is necessary to develop failure criteria for SOFC PEN structures based on the initial flaws occurred during cell sintering and stack assembly. In this paper, the global relationship between the critical energy release rate and critical curvature and maximum displacement of the warped cells caused by the temperature changes as well as mechanical flattening process is established so that possible failure of SOFC PEN structures may be predicted deterministically by the measurement of the curvature and displacement of the warped cells.

1. Introduction

Fuel cells are high-efficiency energy conversion devices that are environmentally friendly with little or no toxic emission. With high efficiency and potential applications in stationary power generation as well as auxiliary power units, solid oxide fuel cell (SOFC) continues to show great promise as a future power source. Among various SOFC designs, anode-supported planar cells seem to provide the best performance at the reasonable cost [1,2]. In anode-supported cells, a porous anode provides the main structural support for the thin (~10 μm) yttria-stabilized zirconia (YSZ) electrolyte layer. The cells must withstand a significant number of thermal cycles with the build-up of internal stresses, which may lead to the cracking of the electrolyte or delamination of the electrolyte–cathode/anode interface [3].

Due to mismatch of the coefficient of thermal expansion (CTE) of various layers in the positive/electrolyte/negative (PEN) structures of SOFC, thermal stresses on the PEN are unavoidable due to the temperature changes from the stress-free sintering temperature to room temperature during the PEN manufacturing process. The stresses in various layers, such as anode, electrolyte, and cathode, may cause the initiation and propagation of cracks. After the sintering processes of PEN structure, cracks were observed in PEN structures of SOFC. The cracks were generated between the electrolyte (YSZ) and fuel electrode (NiO–YSZ) in PEN structure of fuel cells [4,5]. Such thermal internal stresses will also cause cell warpage with a certain curvature. Although various techniques have been developed for sintering the cells, some degree of cell warpage remains after sintering. During stack assembly, the cells with warpage will be flattened, which will contribute to the internal stresses and the initiation and propagation of cracking and delamination. In [6], it was reported that processing-induced residual stresses in the component layers of SOFCs can lead to fracture or to cell curvature which impedes stack assembly. Generally, it has been observed that there are two basic fracture mechanisms occurring in SOFC stacks: delamination along the interface and transverse cracking across the layers [7]. Given the severe thermal cycles that SOFCs must undergo, it is essential to develop suitable materials and design stacks so that they are able to sustain thermo-mechanical loads without cracking.

To ensure the structural integrity of the SOFC stack without cracking and fracture, many efforts have been paid on investigating the fracture behavior of SOFCs and its PEN with the various cracks and flaws by numerical analyses [8–10]. In the numerical fracture analysis, pre-crack has to be formed in the various interfaces of PEN structures and inside various layers, and fine mesh has to be used at the crack tips to capture the stress field of the crack tips in order to obtain the accurate energy release rate. 3D-curved crack in PEN structures was investigated by means of the volume integrals model in [10]. It may be noted that the SOFC PEN is

* Corresponding author. Tel.: +1 509 372 4967; fax: +1 509 372 4672.
E-mail address: wenning.liu@pnl.gov (W.N. Liu).

0378-7753/$ – see front matter © 2009 Elsevier B.V. All rights reserved.
doi:10.1016/j.jpowsour.2009.03.012

Nomenclature

E	Young's modulus
G	energy release rate
G_c	interfacial fracture toughness
H	anode thickness
L	nominal cell size
M	flattening moment
N	resultant forces acting on all the layers
M	resultant moments acting on all the layers
Q	elastic constant matrix
Q	distributed transverse loading
R	curvature radius
ΔT	temperature difference
u	layer displacement in the x-direction
v	layer displacement in the y-direction
w	layer displacement in the z-direction
u_0	displacement of the midplane in the x-direction
v_0	displacement of the midplane in the y-direction
w_0	displacement of the midplane in the z-direction
W	maximum allowable warpage

Greek symbols

α	coefficient of thermal expansion
β	Dundurs parameter
κ	warped cell curvature
ν	Poisson's ratio

characterized by the multilayer thin film structure. A lot of efforts have been contributed in the fracture mechanism of the thin film structures. Interfacial fracture toughness of the thin film structures was experimentally and theoretically studied in [11–16]. The channeling cracks of the thin film and the damage of its propagation on the substrates were investigated deeply for elastic substrate and elasto-plastic substrates in [17–21]. The detailed review is referred to [22]. In these works, energy release rate and stress intensity factors are widely used as criteria of fracture failure, based on the local stress state at the crack tip obtained by the theoretical and numerical analyses.

While being an effective method for the reliability design of SOFC PEN structures, the fracture toughness-based approach described above will have difficulties in predicting failure induced during the sintering and mechanical flattening processes for the SOFC PEN materials. This is because the energy release rate may not be measured directly for the PEN structures of SOFCs during sintering and flattening processes. To ensure the structural integrity and reliability of the SOFC stack, it is necessary to develop a failure criterion for the initial failures that occur during cell–stack assembly.

In this paper, the global failure criteria for PEN fracture are established based on local fracture mechanics formulation for cracks at various locations in the PEN that could be natural result on various interfaces and in cell materials due to the porous nature of the anode and cathode. The critical energy release rate is related to critical curvature and maximum deformation of the warped cells during cell fabrication; therefore the allowable curvature of the warped cells may be calculated, and possible structural failures of the PEN structure can be predicted prior to stack assembly. Specifically, the global failure criteria are formulated based on the warpage of the tri-layer PEN structure, i.e., the cell after sintering process. The warpage of each cell is measured before stack assembly. Then, using the global failure criteria, the engineers can predict whether a cell can survive the stacking assembly process. Clearly, such global failure criteria can also be used for designing the sintering processes to avoid excess warpage of the cells by controlling the pore

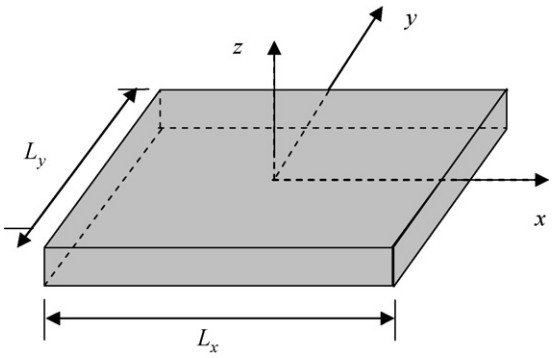

Fig. 1. A functionally graded multiple layer laminate.

size and porosity using the sintering temperature and time as well organic compounds in the PEN structures. The purposes of developing such global failure criteria are to aid the initial design, materials selection, and optimized assembly parameters of SOFC PENs.

2. Basic governing equations of thermal–mechanical analysis of multi-layers and global fracture criterion

2.1. Basic governing equations of thermal–mechanical analysis for functionally graded multi-layers

Consider a multilayered laminate of $L_x \times L_y$, as shown in Fig. 1. The cross-section of the laminate is schematically shown in Fig. 2. The thermo-mechanical properties of each layer may vary layer by layer.

Let u, v and w be the displacements in the x-direction, y-direction and z-direction, respectively. Assuming classical plate bending theory holds and that plane cross-section remains plane, the strain in the laminate can be written as [23]:

$$\varepsilon_x = \frac{\partial u}{\partial x} = \frac{\partial u_0}{\partial x} - z\frac{\partial^2 w_0}{\partial x^2}, \tag{1}$$

$$\varepsilon_y = \frac{\partial v}{\partial y} = \frac{\partial v_0}{\partial y} - z\frac{\partial^2 w_0}{\partial y^2}, \tag{2}$$

$$\gamma_{xy} = \frac{\partial u}{\partial y} + \frac{\partial v}{\partial x} = \frac{\partial u_0}{\partial y} + \frac{\partial v_0}{\partial x} - 2z\frac{\partial^2 w_0}{\partial x \partial y}, \tag{3}$$

where u_0, v_0 and w_0 are the displacements of the middle plane $z = 0$. The preceding strain–displacement relationship can be written in terms of the midplane strains and the plate curvature as follows:

$$\boldsymbol{\varepsilon} = \boldsymbol{\varepsilon}^0 - z\boldsymbol{\kappa} \tag{4}$$

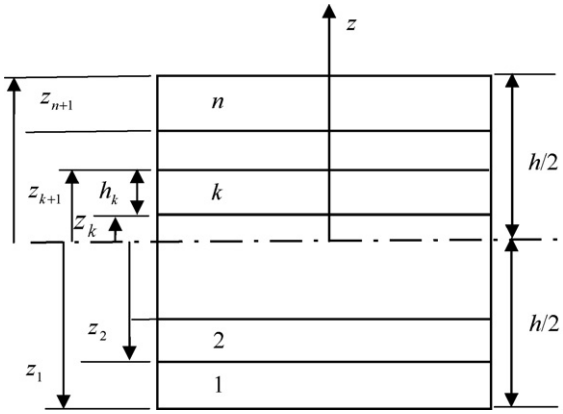

Fig. 2. Cross-section of a multilayer laminate.

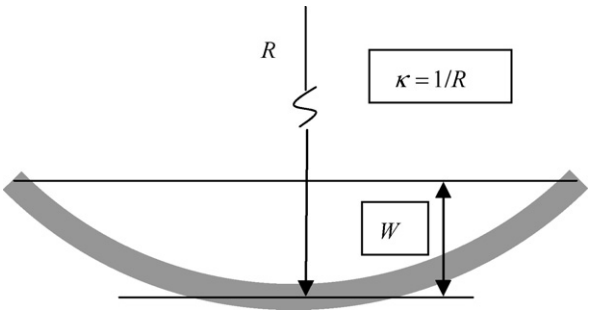

Fig. 3. Illustration of curvature radius *R*.

where

$$\varepsilon^0 = [\varepsilon_x^0, \varepsilon_y^0, \varepsilon_z^0]^{\mathrm{T}} = \left[\frac{\partial u_0}{\partial x}, \frac{\partial v_0}{\partial y}, \frac{\partial u_0}{\partial y} + \frac{\partial v_0}{\partial x}\right]^{\mathrm{T}},$$

$$\boldsymbol{\kappa} = [\kappa_x,\ \kappa_y,\ \kappa_{xy}]^{\mathrm{T}} = \left[\frac{\partial^2 w_0}{\partial x^2},\ \frac{\partial^2 w_0}{\partial y^2},\ \frac{2\partial^2 w_0}{\partial x \partial y}\right]^{\mathrm{T}}.$$

The curvature κ is defined as

$$\kappa = \frac{1}{R}, \tag{5}$$

with radius R shown in Fig. 3, where W denotes the maximum displacement of the multilayer laminate at the center.

Assuming each layer is linear elastic, isotropic, stresses in each layer can be expressed as [24]:

$$\boldsymbol{\sigma} = \mathbf{Q}(\boldsymbol{\varepsilon} - \alpha \Delta T \mathbf{1}), \tag{6}$$

where

$$\boldsymbol{\sigma} = [\sigma_x, \sigma_y, \tau_{xy}]^{\mathrm{T}}, \quad \text{and} \quad \mathbf{1} = [1, 1, 0]^{\mathrm{T}}.$$

and α is the coefficient of thermal expansion (CTE) and ΔT is the temperature change. The above equation can be recast into the following form:

$$\boldsymbol{\sigma} = \mathbf{Q}(\varepsilon^0 - z\boldsymbol{\kappa} - \alpha \Delta T \mathbf{1}), \tag{7}$$

where

$$Q = \begin{bmatrix} Q_{11} & Q_{12} & 0 \\ Q_{12} & Q_{22} & 0 \\ 0 & 0 & Q_{33} \end{bmatrix} = \frac{E}{1-\nu^2} \begin{bmatrix} 1 & \nu & 0 \\ \nu & 1 & 0 \\ 0 & 0 & (1-\nu)/2 \end{bmatrix}$$

with E and ν being the Young's modulus and the Poisson's ratio.

The resultant forces and moments acting on all the layers may be calculated as

$$\mathbf{N} = \int_{-h/2}^{h/2} \boldsymbol{\sigma} dz, \qquad \mathbf{M} = \int_{-h/2}^{h/2} \boldsymbol{\sigma} z dz \tag{8}$$

with

$$\mathbf{N} = [N_x, N_y, N_{xy}]^{\mathrm{T}},$$

$$\mathbf{M} = [M_x, M_y, M_{xy}]^{\mathrm{T}}.$$

Substitution of (7) into (8) yields:

$$\boldsymbol{N} = \boldsymbol{A}\boldsymbol{\varepsilon}^0 - \boldsymbol{B}\boldsymbol{\kappa} - N_0 \mathbf{1}, \tag{9}$$

$$\boldsymbol{M} = \boldsymbol{B}\boldsymbol{\varepsilon}^0 - \boldsymbol{D}\boldsymbol{\kappa} - M_0 \mathbf{1}, \tag{10}$$

where

$$\mathbf{A} = \sum_{k=1}^{n} \int_{z_i}^{z_{i+1}} \mathbf{Q} dz,$$

$$\mathbf{B} = \sum_{k=1}^{n} \int_{z_i}^{z_{i+1}} \mathbf{Q} z\, dz,$$

$$\mathbf{D} = \sum_{k=1}^{n} \int_{z_i}^{z_{i+1}} \mathbf{Q} z^2\, dz,$$

$$N_0 = \sum_{k=1}^{n} \int_{z_i}^{z_{i+1}} \frac{\alpha_i \Delta T E_i}{1-\nu} dz,$$

$$M_0 = \sum_{k=1}^{n} \int_{z_i}^{z_{i+1}} \frac{\alpha_i \Delta T E_i}{1-\nu} z\, dz.$$

Note that for functionally graded materials, both the elastic constant matrix $\mathbf{Q}$ and the CTE α are functions of the coordinate z. Furthermore, if the temperature distribution is not uniform across the thickness, ΔT is also a function of z.

Consider the equilibrium of an infinitesimal element in the laminate, the fact that the total forces and total moment acting on the element must add up to zero provides the following equilibrium equations [25]:

$$\frac{\partial N_x}{\partial x} + \frac{\partial N_{xy}}{\partial y} = 0, \qquad \frac{\partial N_y}{\partial y} + \frac{\partial N_{xy}}{\partial x} = 0, \tag{11}$$

$$\frac{\partial^4 w_0}{\partial x^4} + 2\frac{\partial^4 w_0}{\partial x^2 \partial y^2} + \frac{\partial^4 w_0}{\partial y^4} = -\left(q + N_x \frac{\partial^2 w_0}{\partial x^2} + N_y \frac{\partial^2 w_0}{\partial y^2} + 2N_{xy} \frac{\partial^2 w_0}{\partial x \partial y}\right). \tag{12}$$

where q is the distributed transverse loading, and w_0 represents the z-displacement of the midplane.

With various boundary conditions, the close set of equations will be obtained so that the curvature, displacement and stress in the various layers may be calculated. The several boundary conditions are listed as follows:

Free edge: For a free edge, the bending moment and the shear force must vanish. Thus,

$$M_x(a, y) = 0, \qquad \frac{\partial M_x}{\partial x} + 2\frac{\partial M_{xy}}{\partial y} = 0 \tag{13}$$

Simply supported edge: For a simply supported edge, the deflection and the moment are zero. Thus,

$$w_0(a, y) = 0, \qquad M_x(a, y) = 0 \tag{14}$$

Rigidly clamped edge: In this case, the deflection and the rotation are zero. Thus,

$$w_0(a, y) = 0, \qquad \left.\frac{\partial w_0(x, y)}{\partial x}\right|_{x=a} = 0, \qquad \varepsilon_x^0(a, y) = 0 \tag{15}$$

2.2. Global fracture criteria

Assuming a crack/flaw A exists in a thin film structure as shown in Fig. 4, thermal loading T and/or mechanical loading F will create a corresponding stress field σ, where U represents the deformation field, $\bar{U}$ is the given displacement at the boundary. G refers to the energy release rate at the crack tips.

Stress increase caused by sintering and/or the stack assembly processes may be calculated as

$$\sigma = f(F, E, X), \tag{16}$$

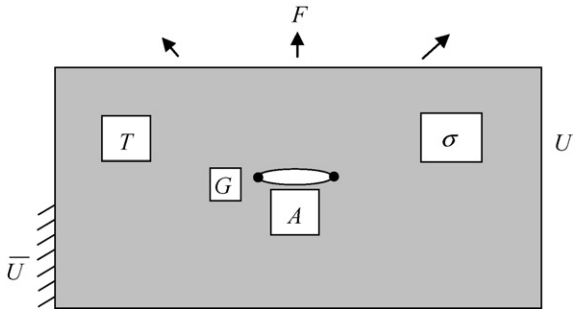

Fig. 4. Illustration of crack, load, stress and deformation.

where E and X represent the mechanical properties of materials and geometry, respectively.

The energy release rate at the crack tip is denoted as G. It is a function of both the mechanical properties E and the geometry X, such that

$$G = g(F, E, X). \tag{17}$$

If this energy release rate exceeds its critical value, G_c,

$$G = g(F, E, X) > G_c, \tag{18}$$

fracture failure occurs. It is a local fracture criterion based on the stress field at the crack tip obtained either numerically, analytically, or experimentally.

In the meantime, the thermal and/or mechanical load F induces deformation of the structure, U, as

$$U = \Psi(F, E, X). \tag{19}$$

Combining Eqs. (18) and (19), the relationship between energy release rate and deformation may be obtained as

$$U = \Psi(g^{-1}(G), E, X). \tag{20}$$

If the relationship given by Eq. (20) is monotonous, the critical deformation U_c can be determined given the critical energy release rate G_c,

$$U_c = \Psi(g^{-1}(G_c), E, X). \tag{21}$$

Therefore, fracture failure will occur if

$$U = \Psi(F, E, X) > U_c = \Psi(g^{-1}(G_c), E, X). \tag{22}$$

Hence, the fracture criterion is based on the global variable, i.e., displacement field, which may be measured easily after the sintering processes of the SOFC PEN structures.

3. Global failure criteria for SOFC PEN

3.1. Thermal residual stress induced deformation of SOFC PEN structures

During the sintering process, SOFC PEN structures are placed in the furnace freely without any constraints on the boundary.

Assuming free edge condition for the PEN boundary at $x = \pm L/2$ and $y = \pm L/2$, the bending moment and the shear force must vanish, which leads to the following set of boundary conditions [25] as boundary condition given in (13):

$$M_x\left(\pm\frac{L}{2}, y\right) = 0, \qquad M_x\left(x, \pm\frac{L}{2}\right) = 0 \tag{23}$$

$$\frac{\partial M_x}{\partial x} + 2\frac{\partial M_{xy}}{\partial y} = 0 \tag{24}$$

The plate curvature due to temperature differential ΔT can be obtained as [24]:

$$\kappa = \Omega \Delta T,$$

where

$$\Omega = \frac{\bar{N}_0(B_{11} + B_{12}) - \bar{M}_0(A_{11} + A_{12})}{(B_{11} + B_{12})^2 - (D_{11} + D_{12})(A_{11} + A_{12})}. \tag{25}$$

with

$$\bar{N}_0 = \sum_{k=1}^{n} \int_{z_i}^{z_{i+1}} \frac{\alpha_i E_i}{1 - \nu}\, dz,$$

$$\bar{M}_0 = \sum_{k=1}^{n} \int_{z_i}^{z_{i+1}} \frac{\alpha_i E_i}{1 - \nu} z\, dz.$$

During stack assembly, the warped cells with curvature κ are flattened by moment M. The relationship between the curvature κ and the flattening moment M is obtained as

$$\kappa = \Omega M. \tag{26}$$

The corresponding stress increase caused by cell flattening can now be calculated as

$$\boldsymbol{\sigma} = z\mathbf{Q}\boldsymbol{\kappa} \tag{27}$$

3.2. Global failure criteria for SOFC PEN

Due to the porous nature of anode and cathode in the PEN structures, initial flaws and crack initiation points will naturally exist on the interfaces of anode/electrolyte/cathode and in the interior of the materials. The types of initial flaws considered here are schematically illustrated in Fig. 5.

Although various techniques have been developed for sintering the cell materials, certain degrees of cell warpage will remain after sintering. During the stack assembly process, cells are flattened in order to fit into the stack. Flattening exerts additional stresses to the warped cells. Such stress may fracture the cell during the flattening process if the warpage is greater than some tolerable level. Therefore, the global failure criteria developed here for PEN structure of SOFCs are based on local fracture mechanics formulations for initial crack size at various location of the cell.

For most anode-supported, YSZ-based SOFCs, the crack types A, B, C and D are particularly vulnerable to the flattening process. The failure criteria below provide a first-order estimate of the maximum allowable warpage and maximum allowable curvature to

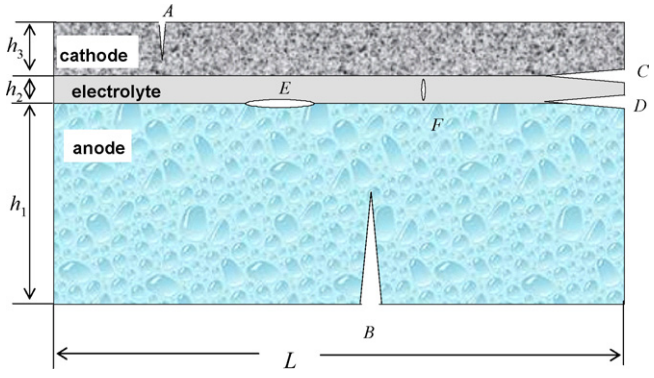

Fig. 5. Cracks at various locations in a cell, where A, surface crack in the cathode; B, surface crack in the anode; C, interfacial crack between the cathode and electrolyte; D, interfacial crack between the anode and the electrolyte; E, blister crack on the anode/electrolyte interface; F, tunneling crack in the electrolyte

avoid fracture during the stack assembly process. In the following context, a is the crack length of each crack type, $E_{a(e,c)}$, $\nu_{a(e,c)}$, $\alpha_{a(e,c)}$ and $h_{a(e,c)}$ represent the Young's modulus, Poisson's ratio, CTE, and thickness of the anode, electrolyte, and cathode, respectively. In addition, subscript *ce* and *ae* stand for the combined properties of cathode/electrolyte composite and anode/electrolyte composite, respectively.

3.3. Crack A

First, we consider the critical curvature the tri-layer PEN structure can withstand during cooling from the sintering temperature, i.e., stress-free temperature to room temperature given the initial flaw *A*.

Based on elasticity theories, the average biaxial stress in the cathode and electrolyte for temperature differential ΔT can be approximated as [22]:

$$\sigma = \frac{E_c}{1-\nu_c}\Delta T\Delta\alpha, \tag{28}$$

where

$$\Delta\alpha = \alpha_c - \alpha_{ae},$$

$$\alpha_{ae} = \frac{\alpha_a E_a h_a + \alpha_e E_e h_e}{\alpha_a h_a + \alpha_e h_e}.$$

Noted that ΔT is the temperature difference from the stress-free temperature to room temperature. Combining Eqs. (25) and (28) yields

$$\kappa = \Omega\frac{1-\nu_c}{E_c\Delta\alpha}\sigma, \tag{29}$$

For stress σ in this crack configuration, the energy release rate may be approximated by the following relations [21]:

$$G = \frac{K^2}{E_c}, \tag{30}$$

where K, the stress intensity factor, is approximated for this type of crack by

$$K = \sigma H$$

$$H = 1.1215\sqrt{\pi a}\left(1-\frac{a}{h_c}\right)^{1/2-s}\left(1+\lambda\frac{a}{h_c}\right).$$

Here a is the initial crack depth, λ is a fitting parameter which is independent of a/h_3 [21], and s is the root of the following equation [26]:

$$\cos(s\pi) - 2\frac{\beta_1-\beta_2}{1-\beta_2}(1-s)^2 + \frac{\beta_1-\beta_2^2}{1-\beta_2^2} = 0. \tag{31}$$

where β_1 and β_2 are the two Dundurs parameters following the work of Dundurs [27]. The relationship of the critical energy release rate G_c and critical curvature κ_c is obtained as

$$G_c = \left(\frac{1}{\Omega}\frac{\Delta\alpha}{(1-\nu_c)}\right)^2 E_c H^2\kappa_c^2, \tag{32}$$

and

$$\kappa_c = \frac{\Omega}{H}\frac{1-\nu_c}{\Delta\alpha}\sqrt{\frac{G_c}{E_c}} \tag{33}$$

For given critical energy release rate G_c, the critical curvature can now be determined.

Next, the energy release rate at the crack tip generated by the flattening process during stack assembly is superimposed on that resulted from the cooling process. Assuming a warped cell with curvature κ is flattened by moment M, the relationship between κ and M can be obtained in Eq. (23) as

$$\kappa = \frac{M(A_{11}+A_{12})}{(B_{11}+B_{12})^2 - (D_{11}+D_{12})(A_{11}+A_{12})}. \tag{34}$$

Assuming free boundary conditions at the edge, the average stress in the cathode may be obtained as

$$\sigma = \frac{h-a}{2}E_c\kappa, \tag{35}$$

where h represents the thickness of the PEN structure. Substitution of Eq. (35) into (30) leads to

$$G = \left(\frac{h-a}{2}\right)^2 E_c H^2\kappa^2. \tag{36}$$

Superimpose the energy release rates from sintering and flattening, i.e., combining Eqs. (33) and (36), one obtains

$$G_c = \left[\frac{1}{\Omega}\frac{\Delta\alpha}{1-\nu_c} + \left(\frac{h-a}{2}\right)\right]^2 E_c H^2\kappa_c^2. \tag{37}$$

For given critical energy release rate G_c, the critical curvature κ_c, is then

$$\kappa_c = \left[\frac{1}{\Omega}\frac{\Delta\alpha}{1-\nu_c} + \left(\frac{h-a}{2}\right)\right]^{-1}\frac{1}{H}\sqrt{\frac{G_c}{E_c}}. \tag{38}$$

3.4. Crack D

Considering the edge crack, Crack D, located in the interface of the anode and electrolyte in the PEN structures. Again, crack tip field generated by cooling is considered first. The cathode and electrolyte in the PEN structure is considered as bi-layer composite plate. For bi-materials laminate, the equivalent elastic modulus, Poisson's ratio, and coefficient of thermal expansion, can be given as [28]:

$$E_{ce} = \frac{h_e E_e + h_c E_c}{h_{ce}}, \tag{39}$$

$$\nu_{ce} = \frac{h_e\nu_e + h_c\nu_c}{h_{ce}}, \tag{40}$$

$$\alpha_{ce} = \frac{\alpha_e h_e E_e + \alpha_c h_c E_c}{h_e E_e + h_c E_c}. \tag{41}$$

The energy release rate may be obtained under the temperature differential as [16]:

$$G = \frac{4h_{ce}}{c_{ce}}F_1(\Delta\alpha)^2(\Delta T)^2, \tag{42}$$

with

$$F_1 = \frac{C_3^2 d_1^2}{I} + \frac{d_2^2}{\Gamma} + 12C_3 d_1 d_2 d_3.$$

The parameters in the above equation are defined in Appendix A as Ref. [26].

From Eqs. (25) and (42), one may obtain the relationship between the energy release rate and the curvature as

$$G = \frac{1}{\Omega^2}\frac{4h_{ce}F_1(\Delta\alpha)^2}{c_{ce}}\kappa^2, \tag{43}$$

therefore,

$$\kappa = \Omega\left[\frac{c_{ce}}{4h_{ce}F(\Delta\alpha)^2}\right]^{1/2}\sqrt{G}. \tag{44}$$

Next, crack tip field resulted by cell flattening during stack assembly is derived. For a cell with curvature κ, the relationship

between the crack tip energy release rate and the curvature and is expressed as

$$G = \frac{c_{ce}F_2}{16h_{ce}^3}\frac{\kappa^2}{\bar{\Omega}^2}, \tag{45}$$

which leads to,

$$\kappa = \bar{\Omega}\left(\frac{16h_{ce}^3 G}{c_{ce}F_2}\right)^{1/2}, \tag{46}$$

where

$$\bar{\Omega} = \frac{A_{11}+A_{12}}{(B_{11}+B_{12})^2-(D_{11}+D_{12})(A_{11}+A_{12})},$$

$$F_2 = \frac{C_2^2}{\Gamma}+\frac{C_3^2}{I}+12C_2C_3d_3.$$

Again, combining the effects of cooling and cell flattening, the relationship of the energy release rate and the curvature can be obtained as

$$G = \left[\frac{1}{\bar{\Omega}}\left(\frac{c_{ce}F_2}{16h_{ce}^3}\right)^{1/2}+\frac{1}{\Omega}\left(\frac{4h_{ce}F_1(\Delta\alpha)^2}{c_{ce}}\right)^{1/2}\right]^2\kappa^2. \tag{47}$$

Using similar derivation process, for each crack type illustrated in Fig. 5, one may derive the relationship between the critical energy release rate and critical curvature of the warped PEN structure as

$$\kappa_c = \bar{Y}\sqrt{\frac{G_c}{h_eE_e}}, \tag{48}$$

where $\bar{Y}$ is dimensionless constant depending on the cell geometry, material constants as well as the size and location of each crack type.

For Crack A,

$$\bar{Y} = \left[\frac{1}{\Omega}\frac{\Delta\alpha}{1-\nu_c}+\left(\frac{h-a}{2}\right)\right]^{-1}\frac{1}{H}\sqrt{\frac{h_eE_e}{E_c}}, \tag{49}$$

and for Crack D,

$$\bar{Y} = \left[\frac{1}{\bar{\Omega}}\left(\frac{c_{ce}F_2}{16h_{ce}^3}\right)^{1/2}+\frac{1}{\Omega}\left(\frac{4h_{ce}F_1(\Delta\alpha)^2}{c_{ce}}\right)^{1/2}\right]^{-1}\sqrt{h_eE_e}. \tag{50}$$

Similarly, the relationship between the critical energy release rate and maximum deformation of the warped PEN structure may be obtained as

$$\frac{W_c}{L} = Y\sqrt{\frac{G_c}{h_eE_e}}\left(\frac{L}{h_e}\right). \tag{51}$$

where W is the maximum allowable warpage, L is the nominal cell size, Y, like $\bar{Y}$, is dimensionless constant, too, depending on the cell geometry, material constants as well as the size and location of each crack type.

4. Illustrative examples

As an example, consider a cell with geometry and material parameters listed in Table 1. For this example, the normal stresses are tensile in the cathode, and compressive in the electrolyte and anode. Therefore, crack types *A*, *C* and *D* may propagate during cell flattening. The values of *Y* for these crack types are listed in Table 2. For $L = 10$ cm, the relationship between the curvature and the energy release rate is depicted in Fig. 6 for various crack types; similarly, Fig. 7 illustrates the relationship between the maximum allowable warpage W and the fracture toughness G_c for these cracks.

Table 1
Material properties and geometric parameters of a cell.

	E (GPa)	ν	CTE ($\times10^{-6}$/°C)	Thickness (μm)
Cathode	90	0.3	11.7	75
Electrolyte	200	0.3	10.8	15
Anode	96	0.3	11.2	500

Table 2
Values of the factor Y ($\times10^{-3}$).

	Crack *A*				Crack *C*	Crack *D*
	$a = 0.01h_3$	$a = 0.05h_3$	$a = 0.1h_3$	$a = 0.2h_3$		
Y	4.63	2.08	1.48	1.06	3.87	2.01

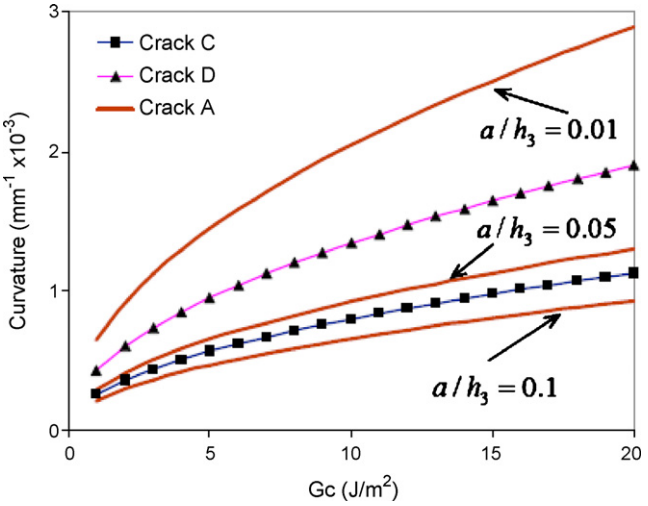

Fig. 6. κ_c vs. G_c for the cell parameters given in Table 1.

It is clear that the critical curvature and maximum allowable deformation for the PEN structure with the surface crack on the cathode will be lowered with the increment of the crack length with given critical energy release rate. Compared with the interfacial edge crack between the anode and the electrolyte, the critical curvature and maximum allowable deformation for the interfacial edge crack between the cathode and electrolyte is much less. The interfacial edge crack between the cathode and electrolyte and the channeling crack in the cathode will be easier to result in fracture failure of the PEN structure after the sintering process and during the cell–stack assembly process. The crack and flaw size in the PEN structure may be controlled by the sintering processes parameter

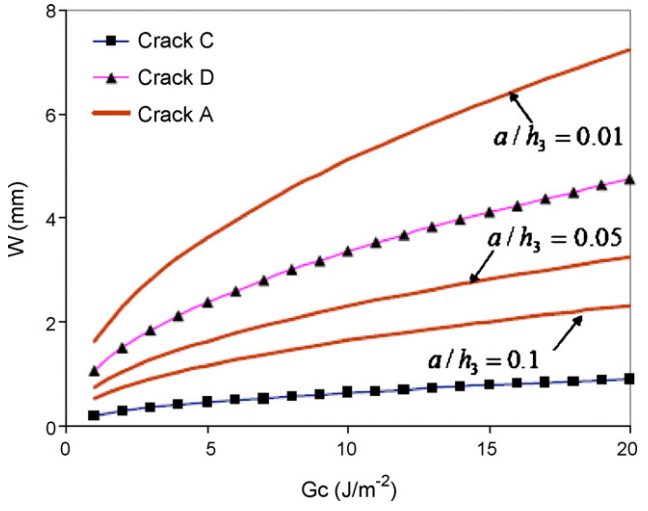

Fig. 7. W vs. G_c for the cell parameters given in Table 1.

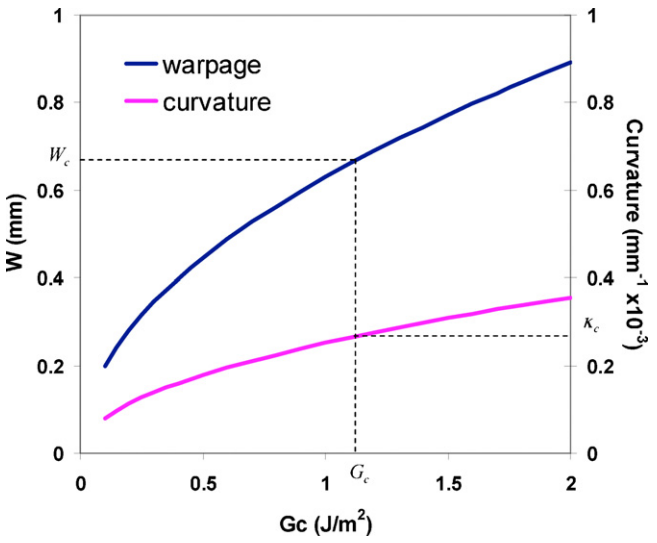

Fig. 8. Relationships between critical curvature and displacement and critical energy release rate.

and the component materials. The process parameter and component materials can be optimized with combination of the fracture failure analysis developed here in order to gain the reliable PEN structure.

For each crack existing in the PEN structure of SOFCs, for a given interfacial strength (i.e., interfacial fracture toughness G_c), the corresponding critical curvature κ_c can be determined. This critical curvature and maximum allowable deformation of the PEN structure will help to judge if PEN structure survives during the cell–stack assembly process pursuing after the sintering process. For example, as shown in Fig. 8 for Crack C, if the curvature and/or the maximum deformation of the PEN structure induced by the sintering process are larger than the critical value obtained here, fracture failure will occur during cell–stack assembly (flattening). Therefore, curvature and/or warpage of the PEN structure may be measured after the sintering process, the PEN structure has to be abandoned if their values of the curvature and/or warpage are larger than the critical value obtained here.

5. Conclusions

In this paper, a suite of global failure criteria for the SOFC PEN structure is derived based on fracture mechanics formulations of local crack tip field for cracks at different locations with different initial sizes. These failure criteria consider the stresses generated from the initial PEN cooling from sintering as well as the mechanical flattening process during stack assembly. The purposes of developing such global failure criteria are to aid the initial design, material selection and optimization of SOFC fabrication process. The critical energy release rate is related to critical curvature and maximum deformation of the warped cells. Since the curvature and displacement of the warped cells can be measured prior to stack assembly, engineers can use the global failure criteria developed here to predict possible failure of a cell structure for various initial crack types. Such global failure criteria can also be used for designing the sintering processes such that allowable warpage and curvature level of the PEN can be achieved for its survival in the subsequent assembly process.

Acknowledgments

This paper was funded as part of the Solid-State Energy Conversion Alliance (SECA) Core Technology Program by the U.S. Department of Energy's National Energy Technology Laboratory (NETL). Pacific Northwest National Laboratory is operated by Battelle Memorial Institute for the U.S. Department of Energy under Contract No. DE-AC05-76RL01830.

Appendix A

$$c_{ce} = \frac{\gamma_{ce}+1}{\mu_{ce}},$$

$$\gamma_{ce} = 3 - 4\nu_{ce},$$

$$\gamma_1 = 3 - 4\nu_1,$$

$$\eta = \frac{h_{ce}}{h_1},$$

$$h_{ce} = h_2 + h_3,$$

$$\Lambda = \frac{\mu_{ce}(\gamma_1+1) - \mu_3(\gamma_{ce}+1)}{\mu_{ce}(\gamma_1+1) + \mu_3(\gamma_{ce}+1)},$$

$$\xi = \frac{1+\Lambda}{1-\Lambda},$$

$$\delta = \frac{1+2\xi\eta+\xi\eta^2}{2\eta(1+\xi\eta)},$$

$$A_0 = \frac{1}{\eta} + \xi,$$

$$I_0 = \frac{1}{3}\left\{\xi\left[3\left(\delta-\frac{1}{\eta}\right)^2 - 3\left(\delta-\frac{1}{\eta}\right)+1\right] + 3\frac{\delta}{\eta}\left(\delta-\frac{1}{\eta}\right) + \frac{1}{\eta^3}\right\},$$

$$C_1 = \frac{\xi}{A_0},$$

$$C_2 = \frac{\xi}{I_0}\left(\frac{1}{\eta} - \delta + \frac{1}{2}\right),$$

$$C_3 = \frac{\xi}{12I_0},$$

$$d_1 = \frac{1}{\eta} - \delta + \frac{1}{2},$$

$$d_2 = 1 - C_1 - C_2 d_1,$$

$$d_3 = \xi\eta^2(1+\eta),$$

$$\Gamma = \frac{1}{1+\xi(4\eta+6\eta^2+3\eta^3)},$$

$$I = \frac{1}{12(1+\xi\eta^3)}.$$

References

[1] A.V. Virkar, J. Chen, C.W. Tanner, J.W. Kim, Solid State Ionics 131 (2000) 189–198.
[2] W.P. Teagan, J.H.J.S. Thijssen, E.J. Carlson, C.J. Read, in: A.J. McEvoy (Ed.), Proceedings 4th European Solid Oxide Fuel Cell Forum, Lucerne, Switzerland, 2000, pp. 969–980.
[3] F. Gutierrez-Mora, J.M. Ralph, J.L. Routbort, Solid State Ionics 149 (2002) 177–184.
[4] R. Okuyama, E. Nomura, Journal of the Ceramic Society of Japan 101 (9) (1993) 1001–1005.

[5] R. Okuyama, E. Nomura, Journal of the Ceramic Society of Japan 101 (4) (1993) 405–409.
[6] O. Kesler, R.L. Landingham, Solid State Ionics—2002. Proceedings of the Mater. Res. Soc. Symposium, vol. 756, 2003, pp. 539–544.
[7] A.N. Kumar, B.F. Sorensen, Mater. Sci. Eng. A 333 (2002) 380–389.
[8] Ba Nghiep Nguyen, B.J. Koeppel, P. Singh, M.A. Khaleel, S. Ahzi, Ceramic Engineering and Science Proceedings, vol. 25, issue 3, 2004, pp. 393–399.
[9] J. Malzbender, R.W. Steibrech, L. Singheiser, Ceramic Engineering and Science Proceedings, vol. 26, issue 4, 2005, pp. 293–298.
[10] J. Johnson, J. Qu, A collection of papers presented at the 30th International Conference on Advanced Ceramics and Composites, 2006, pp. 393–405.
[11] Ran Li, Yu. Shouwen, Materials Science Forum 423–425 (2003) 651–658.
[12] M.R. Elizalde, J.M. Sanchez, J.M. Martinez-Esnaola, D. Pantuso, T. Scherban, B. Sun, G. Xu, Acta Materialia 51 (14) (2003) 4295–4305.
[13] M.B. Modi, S.K. Sitaraman, Engineering Fracture Mechanics 71 (9–10) (2004) 1219–1234.
[14] K.M. Liechti, Y.S. Chai, Transactions of the ASME, Journal of Applied Mechanics 58 (3) (1991) 680–687.
[15] K.M. Liechti, Y.S. Chai, Y.M. Liang, Experimental Mechanics 32 (3) (1992) 218–224.
[16] Z.G. Suo, J.W. Hutchinson, International Journal of Fracture 43 (1990) 1–18.
[17] T. Ye, Z.G. Suo, A.G. Evans, International Journal of Solids and Structures 29 (21) (1992) 2639–2648.
[18] S.S. Chakravarthy, E.H. Jordan, W.K.S. Chiu, Engineering Fracture Mechanics 72 (8) (2005) 1286–1298.
[19] J.M. Ambrico, M.R. Begley, Thin Solid Films 419 (1–2) (2002) 144–153.
[20] M.R. Begley, J.M. Ambrico, International Journal of Fracture 119(4)–120(1–2) (2003) 325–338.
[21] J.L. Beuth, International Journal of Solids and Structures 29 (13) (1992) 1657–1675.
[22] J.W. Hutchinson, Z.G. Suo, Advances in Applied Mechanics 29 (1992) 63–191.
[23] C.E. Turner, Introduction to Plate and Shell Theory, American Elsevier Pub Co., New York, 1965.
[24] E. Ventsel, T. Krauthammer, Thin Plates and Shells: Theory, Analysis and Applications, Marcel Dekker, New York, 2001.
[25] D. Burgreen, Elements of Thermal Stress Analysis, C.P. Press, Jamaica, New York, 1971.
[26] A.R. Zak, M.L. Williams, Journal of Applied Mechanics 30 (1963) 142–143.
[27] J. Dundurs, Journal of Applied Mechanics 36 (1969) 650–652.
[28] A.K. Kaw, Mechanics of Composite Materials, Taylor & Francis, 2006.